RSC Advances

PAPER

Cite this: *RSC Adv.*, 2016, **6**, 51503

Stability and bonding of the multiply coordinated bimetallic boron cycles: $B_8M_2^{2-}$, B_7NM_2 and $B_6C_2M_2$ with M = Sc and Ti†

Hung Tan Pham,[ab] Nguyen Minh Tam,[ab] My Phuong Pham-Ho[c] and Minh Tho Nguyen*[d]

Received 24th February 2016
Accepted 13th May 2016

DOI: 10.1039/c6ra04948f

www.rsc.org/advances

A theoretical investigation of the geometry, stability and aromaticity of boron clusters doped by two Sc and Ti atoms was carried out using DFT calculations. The Sc and Ti atoms form the bimetallic boron cycles not only with the eight-membered ring B_8^{2-} but also with the isoelectronic species B_7N and B_6C_2 rings yielding the planar B_8^{2-}, B_7N and B_6C_2 rings sandwiched to two transition metals. The N and C atoms prefer to form eight-membered hetero-rings *via* the classical 2e–2c bonding rather than occupy high coordination positions. Both C atoms avoid binding each other. The thermodynamic stability of all bimetallic boron cycles is induced by the stabilizing overlap between the bonding and anti-bonding MOs of a metallic dimer M_2 with levels of an eight-membered ring. These stabilizing interactions also release two sets of delocalized σ and π MOs, which obey the $(4N + 2)$ electron count. Such a double σ and π aromaticity feature is clearly supported by the magnetic ring current flows.

1. Introduction

The diversity in geometrical structures of small boron clusters is bewildering. While it is well known that the B_{12} icosahedral three-dimensional (3D) cage is a structural unit in many boron polyforms,[1] this structure is found to be much less stable than its planar isomer.[2] Previous studies on a large number of pure boron clusters show that the bare boron clusters basically have four different classes of structures involving the planar (or quasi-planar), the tubular (double ring, triple ring and multiple ring…), the bowl shaped, and the fullerene-like and cage forms. Most of the boron clusters B_n having sizes smaller than $n < 20$ atoms are planar or quasi-planar,[3] whereas the lowest-lying structures of the even sizes B_{2m} in the range of $2m = 20$–26 have a double ring form. The latter is the simplest tubular structure, which consists of two B_m strings often connected in an anti-prism fashion.[4] The triple ring form is observed in B_{27} and B_{42} which result from a superposition of three B_9 and B_{14} strings in an anti-prism motif, respectively.[5,6] Regarding the cationic state, 3D structure is already found for the size of B_{17}^+ (ref. 7) whereas the planar and quasi-planar forms remain the global minimum structures for anionic boron clusters up to the size of B_{27}^-.[5,8] The B_{30}, B_{32} and B_{36} clusters present the bowl shape which contains a large hole, and their electron distribution satisfies the disk-aromaticity.[6,9,10] A fullerene motif of structure is established in the case of B_{38} and B_{40} clusters.[11–13] Recently, the B_{44} cluster has been shown to have a cage-like structure containing two nonagonal holes. Such a feature is unprecedented in elemental clusters.[14]

Another class of boron clusters, represented firstly by the anions B_8^{2-} and B_9^-, has planar cyclic geometry in which a B atom occupies the central position of the B_7 and B_8 rings, respectively.[15] It is remarkable that a doping of one transition metal M gives rise to the M@B_n planar cyclic structures in which the M atom is surrounded by the B_8, B_9 and B_{10} rings.[8] The stability of the planar metallic boron cycles can be rationalized in terms of strong orbital interactions where the transition metal uses its d-AOs to form two delocalized bonding patterns. The latter satisfy the classical $(4N + 2)$ electrons count in both series of delocalized π and σ MOs therefore they are classified as doubly π and σ aromatic. Stimulated by the finding that the $B@B_5H_5^+$ cluster is a planar cycle,[16] in which one B atom occupies the central position of the $B_5H_5^+$ pentagonal cycle, a number of doped $M@B_nH_n$ cyclic forms have been established.[17] The planarity of these systems are rationalized by the aromaticity with 10 π electrons. Although several boron rings centered by other main group elements were previously investigated, none of them was found to be a global minimum on the corresponding potential energy surface.[18,19] The central atom needs to form delocalized π and σ bonds with the B_n ring, but

[a]*Computational Chemistry Research Group, Ton Duc Thang University, Ho Chi Minh City, Vietnam. E-mail: phamtanhung@tdt.edu.vn*

[b]*Faculty of Applied Sciences, Ton Duc Thang University, Ho Chi Minh City, Vietnam*

[c]*Institute for Computational Science and Technology (ICST), Ho Chi Minh City, Vietnam*

[d]*Department of Chemistry, KU Leuven, Celestijnenlaan 200F, B-3001 Leuven, Belgium. E-mail: minh.nguyen@kuleuven.be*

† Electronic supplementary information (ESI) available. See DOI: 10.1039/c6ra04948f

when a main group element having a larger electronegativity than B, it favors connection to other atoms through simpler 2 center–2 electrons (2c–2e) bonds. As for typical examples, carbon–boron mixed cluster reveals many $B@B_xC_y$ boron hetero-cycles where C atoms participate to ring not in central position.[20–23] The electronic partition analysis shows that C atoms provide to the delocalized π and σ MOs and subsequently stabilize boron cycles.

For the boron-based clusters multiply doped by transition metal atoms, some organometallic compounds were observed. In the series of bimetallic complexes $B_nX_nRe_2$, the boron ring is uniformly coordinated with two Re atoms. Of the derivatives B_5X_5 and B_6X_6, the boron units were found to be perfectly planar pentagon and hexagon motifs, respectively.[24,25] The planar B_6 ring was found to play as a key structural motif in the solid compound $Ti_7Rh_4Ir_2B_8$,[26] in which the B_6 unit is sandwiched by two Ti atoms. Recently, we reported on a novel motif of structure in which two metals are coordinated vertically and oppositely with the planar boron ring.[18] In these bimetallic boron cycles having Fe and Co as dopants, the global energy minima of the resulting B_7Co_2, B_7Fe_2 and B_7CoFe clusters contain each a perfectly planar B_7 cycle, which is sandwiched with two metallic atoms vertically placed along the C_7 axis.[27] The high thermodynamic stability of these bimetallic boron cycles arises from a combination of two stabilizing effects. On the one hand, the M_2 dimeric metals introduce their electrons to fill up the empty levels of the B_7 string, and on the other hand, both anti-bonding and bonding MOs of M_2 are significantly stabilized through orbital interactions with the cyclic B_7 counterpart.

Although bimetallic boron clusters have been identified in the seven-membered boron rings with Fe and Co as dopants, the derivatives containing larger boron rings such as eight-membered ring are not known yet. As mentioned above, the main group elements such as the C and N atoms tend to prefer formation of classical 2c–2e bonds, in part due to their higher electronegativity. As a prediction, these atoms possibly connect with boron atoms to reveal hetero-cycles and subsequently, in the presentation of metals, the bimetallic hetero-boron cycles could be established. In this context, we set out to search for new members of the family of bimetallic boron cycles containing eight-membered rings using quantum chemical computations. Our extensive theoretical search on the geometry and electronic structure of several B_8M_2 species reveals that the M = Sc and Ti atoms are quite suitable for this purpose. For the eight-membered rings, beside the neutral B_8 and its dianionic B_8^{2-} ring, simple substitutions generating the B_7N ring (with substitution of B^{2-} by N) and the B_6C_2 ring (with replacement of two B^- anions by two C atoms) are also considered. The latter systems allow us to analyze the behavior of the series of isoelectronic systems. The electronic structure and chemical bonding feature of this class of bimetallic boron cycles will be examined using the electron localization indicator. Their aromatic character is further probed using the magnetic response of the electron density as described by the ring current maps.

2. Computational methods

The potential energy surfaces of the B_8M_2, $B_8M_2^{2-}$, B_7NM_2 and $B_6C_2M_2$ clusters, with M = Sc and Ti, are explored using the stochastic genetic algorithms.[28] In addition, the guess structures are also manually built by adding two metal atoms to the framework of the pure B_n species. Initial B_7NM_2 and $B_6C_2M_2$ structures obtained following substitution of a single B atom by a N, or two B atoms by two C are also generated on the basis of the $B_8M_2^{2-}$ counterparts.

Geometric optimizations and harmonic vibrational analyses are carried out using density functional theory (DFT) with the hybrid TPSSh,[29] which was previously shown to give better results on relative energies for boron clusters than those obtained with other available functionals, as compared to the high accuracy MO coupled-cluster method (CCSD(T)).[30] The PBE1PBE[31] and BPW91 (ref. 32) functionals are found to excellently predict geometry and spin state of $Fe(C_6H_6)_n$ systems,

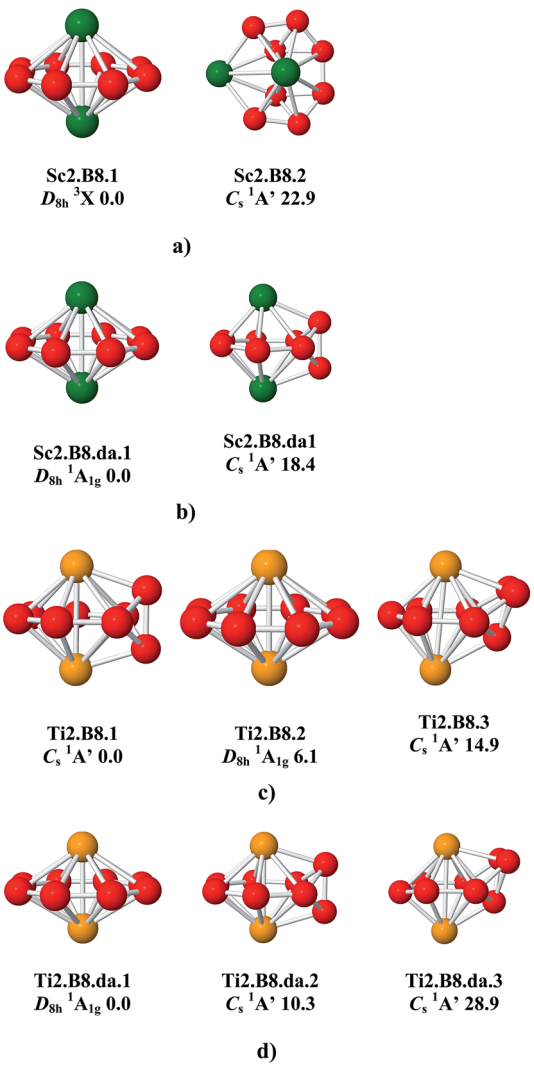

Fig. 1 Energetically lower-lying isomers of (a) B_8Sc_2, (b) $B_8Sc_2^{2-}$, (c) B_8Ti_2 and (d) $B_8Ti_2^{2-}$ clusters. Geometry optimizations and relative energies (kcal mol^{-1} with ZPE corrections) were obtained using the TPSSh/cc-pVTZ computations.

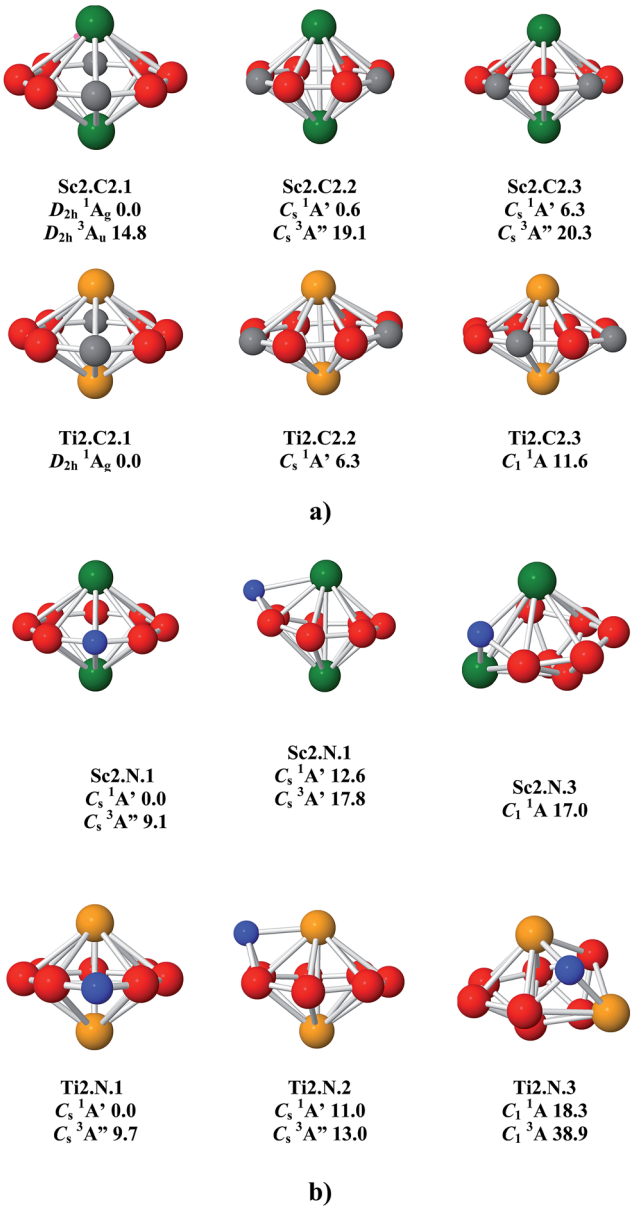

Fig. 2 Lower-lying isomers of (a) $B_6C_2Sc_2$ and $B_6C_2Ti_2$ clusters, and (b) B_7NSc_2 and B_7NTi_2 clusters. Geometry optimizations and energies (kcal mol^{-1} with ZPE corrections) were performed using the TPSSh/cc-pVTZ computations.

therefore these functional are use in the current investigation where the B_6C_2 and B_7N containing structures are considered.[33] In order to evaluate the reliability of three functionals, the bond length, vibrational frequency, dissociation energy and electron affinity (EA) of the dimers Sc_2 and Ti_2 are calculated and compared to available experimental values.[34–40] As shown in Table 1, in comparison to available experimental values, the TPSSh and PBE1PBE in combining with the cc-pVTZ basis set produce better results than the BPW91/cc-pVTZ calculation.

The initial structures are first optimized using the small 3-21G(d) basis set.[41,42] The optimized lower-energy isomers, being within a range of 50 kcal mol^{-1} on relative energies, are subsequently reoptimized using the same TPSSh functional, but in conjunction with the larger cc-pVTZ basis set.[43,44] Electronic structure theory computations are performed using the Gaussian 09 suite of program.[45]

The magnetic response is calculated using the CTOCD-DZ method[43] implemented in the SYSMO program,[46,47] which is connected to the GAMESS-UK package.[48] The ring current approach[49,50] is calculated using the B3LYP/6-311G(d) level. In the current density map, the contour and shading show the modulus of induced current density and narrows display its projection on plotting plane. As for a convention, anticlockwise or clockwise circulations correspond to diatropic or paratropic current, respectively. The diatropic current flow indicates an aromatic character, whereas the paratropic current flow suggests an anti-aromatic character.

3. Results and discussion

3.1 Geometries of the B_8M_2, $B_8M_2^{2-}$, B_7NM_2 and $B_6C_2M_2$ clusters

Only the eight-membered boron cycles are considered in this investigation. As for a convention, the structure is noted as **M2.X.*n***, in which M2 = Sc2 and Ti2 stands for two metal dopants, X = B8, C2 and N according to the pure B_8 cycle and the substituted derivatives by two and one B atoms by two C and one N atoms, respectively, and finally n = 1, 2, 3… denotes the isomers with increasing energy ordering. When relative energies are mentioned, the values are consistently referred to the corresponding most stable isomer n = 1. In the dianionic $B_8M_2^{2-}$, the isomers are referred to as **M2.B8.da.*n***.

Fig. 1 displays the shape of the energetically lower-lying isomers of both series B_8M_2 and $B_8M_2^{2-}$ with M = Sc and Ti obtained using the TPSSh/cc-pVTZ level. Geometry of $B_6C_2M_2$ and B_7NM_2 are displayed in Fig. 2. As for a comparison, their relative energy obtained by using three different TPSSh, PBE1PBE and BPW91 functionals in various spin states are listed in Table 1.

Table 1 Bond length (d(M_2), angstrom), vibrational frequency (Freq., cm^{-1}), dissociation energy (D_o, eV) and electron affinity (EA, eV) of Sc_2 and Ti_2 obtained by TPSSh, PBE1PBE and BPW91 calculations and compared to experiment (Exptl)

	Exptl			TPSSh				PBE1PBE				BPW91			
	d(M_2)	Freq.	D_o	d(M_2)	Freq.	EA	D_o	d(M_2)	Freq.	EA	D_o	d(M_2)	Freq.	EA	D_o
Sc_2	2.51[a]	238.9[c]	1.65[e]	2.6	258.3	0.68	1.1	2.6	267.3	0.94	0.76	2.6	241.3	2.9	−0.5
Ti_2	1.94[b]	407.9[d]	1.54[f]	1.90	502.3	0.35	2.0	1.95	536.8	1.0	1.2	1.90	470.7	0.7	2.2

[a] CASSCF calculations taken from ref. 33. [b] Ref. 36 and 37. [c] Ref. 35. [d] Ref. 38. [e] Ref. 39. [f] Ref. 40.

Table 2 The relative energy (kcal mol^{-1}) of B_8M_2, $B_8M_2^{2-}$, $B_6C_2M_2$ and B_7NM_2 clusters with M = Sc and Ti at various spins states using TPSSh, PBE1PBE and BPW91 functionals combining with cc-pVTZ basis set

	TPSSh			PBE1PBE			BPW91		
Structure	Singlet	Triplet	Quintet	Singlet	Triplet	Quintet	Singlet	Triplet	Quintet
Sc2.B8.1	3.4	0.0	48.7	4.0	0.0	48.0	4.0	0.0	44.3
Sc2.B8.2	22.9	47.5	68.7	22.3	46.0	66.3	22.2	38.1	60.6
Ti2.B8.1	0.0	15.5	41.8	0.0	21.8	41.8	0.0	15.4	42.0
Ti2.B8.2	6.1	6.4	11.8	10.1	9.5	11.4	5.7	7.7	15.9
Ti2.B8.3	14.9	18.8	42.6	15.0	17.6	38.3	12.5	17.7	43.2
Sc2.B8.da.1	6.8	15.2	0.0	12.3	0.0	16.8	15.0	0.0	4.2
Sc2.B8.da.2	25.1	20.3	31.3	38.7	27.3	33.1	33.4	26.1	33.6
Ti2.B8.da.1	0.0	3.5	0.5	0.5	0.0	0.0	0.0	15.9	6.9
Ti2.B8.da.2	10.3	9.0	17.8	8.3	1.1	27.0	9.4	6.7	18.5
Ti2.B8.da.3	28.9	20.4	23.4	26.7	16.2	22.4	27.0	19.5	23.4
Sc2.C2.1	0.0	15.7	49.7	0.0	16.0	45.7	0.0	14.5	47.3
Sc2.C2.2	0.6	20.2	45.2	0.5	20.6	45.7	0.7	18.7	43.4
Sc2.C2.3	6.5	22.6	47.0	6.6	22.3	47.5	6.1	19.5	45.3
Ti2.C2.1	0.0	6.8	11.0	0.0	4.0	6.0	0.0	1.5	14.1
Ti2.C2.2	6.6	4.2	17.5	6.8	1.5	12.6	6.2	6.0	16.5
Ti2.C2.3	12.1	6.1	16.4	12.0	12.1	11.7	10.2	7.4	18.8
Sc2.N.1	0.0	10.1	34.3	0.0	8.2	35.6	0.0	8.9	32.0
Sc2.N.2	13.1	18.4	46.7	11.3	17.7	36.3	11.9	17.1	35.7
Sc2.N.3	22.5	41.0	71.9	20.8	39.4	74.3	21.1	40.3	68.1
Ti2.N.1	0.0	10.6	19.0	0.0	14.3	14.1	0.0	15.1	26.2
Ti2.N.2	11.6	14.6	38.6	10.5	10.7	27.8	14.6	17.5	41.7
Ti2.N.3	18.7	40.0	43.1	17.8	34.7	36.5	21.7	41.1	51.0

For the neutral B_8Sc_2 cluster, the triplet spin state **Sc2.B8.1** is confirmed as the ground state by TPSSh, PBE1PBE and BPW91 calculations whereas the quintet multiplicity is highly unstable. The structural characteristic of **Sc2.B8.1** shows that two Sc atoms are vertically coordinated to the planar B_8 string. All DFT calculations demonstrate that the next isomer **Sc2.B8.2**, in three spin states, is extremely unstable. In the following section, the structural motif in which two metal atoms are vertically sandwiched in the opposite sides of a planar eight-membered ring is referred to as a 'bimetallic planar cyclic cluster'. Following attachment of two electrons, the bimetallic cyclic structure **Sc2.B8.da.1** is also found to be the lowest energy isomer. TPSSh/cc-pVTZ calculations point out that the quintet multiplicity is the ground state of **Sc2.B8.da.1**, whereas both PBE1PBE/cc-pVTZ and BPW91/cc-pVTZ computations predict the triplet spin state as the ground state. The fish-like structure **Sc2.B8.da.2** is predicted to be highly unstable by all DFT calculations (Table 1).

The boron cyclic form is not favored in the neutral B_8Ti_2. The fish-like structure **Ti2.B8.1** (C_s $^1A'$) in which both metal atoms are coordinated to a B_6 string and two B atoms capped at two different sites of the same B–B edge, is the ground state of B_8Ti_2. The **Ti2.B8.2** bimetallic cycle (D_{8h} $^1A_{1g}$) is much less stable as indicated by TPSSh, PBE1PBE and BPW91 calculations (Table 1). However, the bimetallic boron cycle **Ti2.B8.da.1** turns out to be again the lowest-energy structure for the dianion $B_8Ti_2^{2-}$, being ~10 kcal mol^{-1} below the corresponding fish-like structure (Table 1). It should be stressed that both Sc and Ti dopants give rise to the bimetallic cyclic boron structures with high symmetry in the dianion state.

Similar to the $B_8Ti_2^{2-}$ and $B_8Sc_2^{2-}$ dianions, both isoelectronic neutral $B_6C_2Sc_2$ and $B_6C_2Ti_2$, where the two B^- centers of B_8 are replaced by two C atoms, remain stable in the bimetallic cyclic motif with the emergence of a B_6C_2 planar heterocycle. In the case of $B_6C_2Sc_2$, the TPSSh, PBE1PBE and BPW91 calculations show that the singlet **Sc2.C2.1** and **Sc2.C2.2** isomers are degenerate with an energy gap of <1 kcal mol^{-1}, and as a consequence they can be regarded as competing ground state for the neutral mixed $B_6C_2Sc_2$. Within these structures, two Sc atoms are coordinated vertically but oppositely to the B_6C_2 perfect planar ring.

Similar structure is observed also in the case of Ti-dopant. As shown in Fig. 2a, a hetero-boron cycle structure, **Ti2.C2.1**, is identified as the ground state of $B_6C_2Ti_2$ with high symmetry and low spin multiplicity (singlet state) by all functionals used.

Table 3 The dissociation energy of bimetallic cycles obtained by TPSSh, BPW91 and PBE1PBE calculations

	TPSSh	BPW91	BPE1PBE
$B_8Sc_2 \rightarrow B@B_7 + Sc_2$	230.8	289.7	224.6
$B_8Sc_2^{2-} \rightarrow B@B_7^{2-} + Sc_2$	174.8	216.0	171.5
$B_8Ti_2 \rightarrow B@B_7 + Ti_2$	218.9	306.9	215.2
$B_8Ti_2^{2-} \rightarrow B@B_7^{2-} + Ti_2$	165.0	232.9	156.9
$B_8Sc_2 \rightarrow B_8 + Sc_2$	328.0	312.0	333.5
$B_8Sc_2^{2-} \rightarrow B_8^{2-} + Sc_2$	332.1	271.2	288.3
$B_8Ti_2 \rightarrow B_8 + Ti_2$	327.4	406.6	334.9
$B_8Ti_2^{2-} \rightarrow B_8^{2-} + Ti_2$	286.5	299.7	289.8
$B_7NSc_2 \rightarrow B_7N + Sc_2$	286.8	271.1	289.0
$B_7NTi_2 \rightarrow B_7N + Ti_2$	259.9	257.9	261.1
$B_6C_2Sc_2 \rightarrow B_6C_2 + Sc_2$	305.5	289.7	309.5
$B_6C_2Ti_2 \rightarrow B_6C_2 + Ti_2$	279.4	272.5	282.2

Some other bimetallic boron cycles are observed on the potential energy surface of $B_6C_2Ti_2$, but they are significantly less stable than **Ti2.C2.1**. It is remarkable that the bimetallic boron cycles $B_6C_2M_2$ with M = Sc and Ti containing C–C connection are highly unstable, which results from the fact that in the formation of bimetallic carbon–boron cycles with two C atoms, the C dopants avoid to meet and to bind to each other.

Substitution of a single B site of $B_8Sc_2^{2-}$ and $B_8Ti_2^{2-}$ by an N atom also releases a bimetallic cyclic structure, **Sc2.N.1** and **Ti2.N.1** again with a planar B_7N hetero-ring. The fish-like structures **Sc2.N.2** and **Ti2.N.2** are found at ~10–14 kcal mol^{-1} above the corresponding ground state, predicted by TPSSh, PBE1PBE and BPW91 calculations, respectively. The next isomers **Sc2.N.3** and **Ti2.N.3** are highly unstable in both singlet, triplet and quintet states.

Overall, the dianion $B_8M_2^{2-}$ with M = Sc and Ti and their isoelectronic neutral $B_6C_2M_2$ and B_7NM_2 clusters provide us with the new members of the class of bimetallic boron cycles. Of these species, it is clear that **Sc2.C2.1**, **Sc2.N.1**, **Ti2.C2.1** and **Ti2.N.1** present the bimetallic hetero-boron cycles in which two metals are coordinated to B_6C_2 and B_7N hetero-ring. The most interesting result here is that both N and C atoms participate together with boron atoms in the formation of the eight-membered hetero-ring rather than to be located in highly coordinated position as the two metals.

3.2 Energetic properties

In order to explore the stability of bimetallic boron cycles, the dissociation energy (DE) where parent structure dissociates giving a metallic dimer plus the corresponding ring, is calculated using three functionals and given in Table 3. Additionally, the binding energy (BE, Table 4) are also performed to quantify their stability. The DE values of the channel in which B_8M_2 and $B_8M_2^{2-}$ structures release the global minimum B_8 and B_8^{2-} plus M_2 dimers, are significantly lower (Table 2) and illustrates that B_8M_2 and $B_8M_2^{2-}$ favor the dissociation channel giving B@B_7 and B@B_7^{2-}. The DE value of the $B_8M_2^{2-}$ dianion is somewhat lower than that of the neutral. The connection between M_2 and B_8^{2-} dianionic ring becomes thus weaker than that between M_2 and B_8 neutral ring. This is supported by binding energy calculations in which BE value of neutral B_8M_2 is greater than the corresponding $B_8M_2^{2-}$. Similarly, in comparison to B_8M_2 neutral, DE values of B_7NM_2 and $B_6C_2M_2$ cluster with M = Ti and Sc are smaller, therefore the interactions between M_2 and B_7N and B_6C_2 rings are weaker than that of in the B_8M_2 neutral. Although the substitution of B atom by N and C atoms in B_8^{2-} ring results in many new BN, CB bonds which are stronger than the BB bond in B_8^{2-} ring, the interactions of two M atoms with the rings either in B_7NM_2 and $B_6C_2M_2$ or in B_8M_2 and $B_8M_2^{2-}$ cycles are of the same order of magnitude.

It should be noted that although the B_8Ti_2 bimetallic cycle is not the global minimum, this structure has a greater DE value than $B_8Ti_2^{2-}$ cycle which is determined as the ground state. In combination with calculations of the binding energy, these results show that the interaction of M_2 dimer with B_8, B_8^{2-}, B_7N and B_6C_2 rings which is one main contributor to the stability of bimetallic boron cycles, is quantitatively comparable. The delocalization or aromaticity is more important in stability, particular for di-anions $B_8M_2^{2-}$, B_7NM_2 and $B_6C_2M_2$ cycles, as shown in following sections.

Table 4 The binding energy (D_0, kcal mol^{-1}) of bimetallic cycles obtained. Using three different functionals with the cc-pVTZ basis set

	TPSSh	BPW91	PBE1PBE
B_8Sc_2	106.8	110.1	109.3
$B_8Sc_2^{2-}$	104.8	108.8	107.8
B_8Ti_2	107.7	111.4	109.3
$B_8Ti_2^{2-}$	105.9	110.0	107.3
B_7NSc_2	115.5	114.9	118.0
B_7NTi_2	117.0	117.0	118.3
$B_6C_2Ti_2$	126.0	130.0	127.6
$B_6C_2Sc_2$	125.5	129.2	128.4

3.3 Metal–metal bonding

For an understanding on the behavior of the two metallic atoms, the Wiberg bond indexes (WBI)[51,52] are performed for both free metal dimers, and the M–M bonds in bimetallic boron cycles, and the calculated results are given in Table 5. The bond lengths of the free diatomic Sc_2 and Ti_2 amount to 2.8 and 1.94 Å,[53] respectively, and WBI values are found as 0.25 and 0.78. As seen from Table 5, the bond lengths calculated for the M_2 connection in all bimetallic boron cycles including $B_8M_2^{2-}$, B_6C_2M and B_7NM_2 is ~0.5 Å longer than those of free metal dimers, while the WBI values of M–M connections change according to the nature of the dopant. The $B_8M_2^{2-}$ clusters have WBI values of ~0.6 for Ti_2 and Sc_2, but these are of 0.9 and 0.5 for B_7NTi_2 and B_7NSc_2 clusters, respectively. For $B_6C_2M_2$, WBI values amount to 1.2 and 0.5 for Ti and Sc dopants, respectively. On the geometrical aspect, formation of bimetallic boron cycles tends to increase distance between two metal atoms. Although

Table 5 Bond length of M–M, B–M, C–M, N–M, C–B and N–B (Å) and WBI values of M–M connections of the bimetallic boron cycles

Species	Parameter	Ti	Sc
M_2	d(Exptl)	1.94	2.51
	d(M_2)	1.90	2.6
	WBI	0.78	0.25
$B_8M_2/B_8M_2^{2-}$	d(M–M)	2.92, 2.49	2.94, 2.83
	d(B–M)[a]	2.4	2.4
	WBI	0.64	0.65
B_7NM_2	d(M–M)	2.7	2.9
	d(B–M)	2.3	2.4
	d(N–M)	3.0	2.3
	d(N–B)	1.4	1.4
	WBI_{M-M}	0.9	0.49
$B_6C_2M_2$	d(M–M)	2.5	2.9
	d(B–M)	2.3	2.4
	d(C–M)	2.4	2.3
	d(C–B)	1.4	1.4
	WBI_{M-M}	1.2	0.48

[a] Value obtained for $B_8M_2^{2-}$ cyclic structure.

the WBI value of M_2 in $B_8M_2^{2-}$ is reduced, the $B_6C_2M_2$ and B_7NM_2 result in larger values of WBI for the M_2 unit. According to the meaning of WBI, the presence of C or N dopants tends to enhance the strength of M–M bonds, in spite of their longer distances.

3.4 Orbital interactions

To probe further the chemical bonding feature and thereby the stability of bimetallic boron cycles, it is imperative to consider the bonding model which raises from d–d interactions.[54] As for a representative example, Fig. 3 illustrates the orbital interactions of the Ti_2 dimer with the B_8^{2-} string. The results obtained for Ti_2 can be generalized for others bimetal-doped boron cycles.

The Ti atom has an electron configuration of $[Ar](3d)^2(4s)^2$, and as a consequence, the Ti_2 dimer has enough electrons to fully occupy an electronic configuration of $[\sigma_{4s}^2\sigma_{3d}^2\pi^4]$. The two σ MOs include the σ_{4s} orbital which is resulted from overlap of the 4s AOs, and the σ_{3d} which is a combination of 3d AOs. The anti-bonding δ*, π* and σ* MOs are filled, and thereby, the strength of metal–metal bond is reduced.

The delocalized MO pattern of the ring B_8^{2-} appears to satisfy a disk aromatic framework, which arises from a model of a particle in a circular box.[55] Within this model, the boundary condition gives two quantum numbers, namely the radial quantum number n and the rotational quantum number m. The radial quantum number has values of $n = 1, 2, 3, \ldots$ whereas $m = 0, \pm1, \pm2, \ldots$ which is denoted as $m = \sigma, \pi, \delta, \ldots$, respectively. The state with non-zero value of m shall thus be doubly degenerate. The lowest-lying eigenstates in ascending energy are 1σ, 1π, 1δ… *etc.* The full occupation of degenerate eigenstates which correspond to 2, 6, 12, 16, 20, … electrons leads to a disk aromatic character.

The orbital interaction of the B_8^{2-} disk configuration and the Ti_2 bond inherently enhances the stability of boron cycles, as displayed in Fig. 3. From there, the π*-MOs of the Ti_2 dimer whose occupation significantly reduces the strength of the Ti–Ti bond, are stabilized upon interaction with the doubly degenerate 1π levels of either the ring B_7^- or B_8, and thereby produces the π levels of the entire system. Interestingly, the δ*-MOs of Ti_2 enjoy a stabilizing overlap with the vacant 1δ level, and releases the doubly degenerate δ* levels, as given in Fig. 3. Interaction of the bonding σ_{4s} and the 2σ level ends up in a creation of the σ_{4s} MOs for the $B_8Ti_2^{2-}$ bimetallic dianion. The π bonding MOs of Ti_2 have an enhanced overlap with the 2π level of the B_8^{2-} disk, whereas the 2δ-MOs of the B_8^{2-} counterpart undergo a stabilizing interaction with the δ-MOs of Ti_2 yielding the δ levels of the complex. As a result, the orbital configuration of the $B_8Ti_2^{2-}$ cyclic structure as $[\ldots(\sigma_{4s})^2(\pi)^4(\pi^*)^4(\delta)^2(\delta^*)^4]$ is now fully occupied by 16 electrons.

The electron configurations of the different bimetallic cyclic boron clusters are listed in Table 6. The π* and δ* levels of the isoelectronic cycles to $B_8Ti_2^{2-}$ involving $B_6C_2Ti_2$ and B_7NTi_2 are fully occupied (Table 6). As a result, they tend to enhance the stability of cyclic structures, although they reduce the strength of Ti–Ti connection. The σ_{4s} and π levels are actually fully occupied, whereas the δ molecular orbitals are filled by two (2) electrons. These MOs increase the strength of Ti–Ti bond, and stabilize consequently the bimetallic cyclic boron clusters. The dianion $B_8Sc_2^{2-}$ has the orbital configuration of $\ldots(\sigma_{4s})^2(\pi^*)^4(\pi)^4(\delta^*)^4$ in which the π* and δ* MOs are fully occupied, as given in Table 2. The π* and δ* MOs of the isoelectronic boron cycles with $B_8Sc_2^{2-}$ involving B_7NSc_2 and $B_6C_2Sc_2$ are also fulfilled by 4 electrons for each cluster. It is obvious that they are significant contributor to the stability of boron cycles containing the Sc-dopant. The full occupation of σ_{4s} and π levels contributes significantly to the thermodynamic stability of cyclic structure, due to the enhanced Sc–Sc connection. Therefore, a successive occupation of σ_{4s}, π, π* and δ* levels leads to the formation of bimetallic boron cycles. It is clear from Table 6 that the $B_6C_2Ti_2$ and B_7NTi_2 have different MO patterns, in which the appearance of C and N atoms, that are more electronegative than B atom, leads to a substantial change in the MO energy levels with expected splitting of the doubly degenerate MOs.

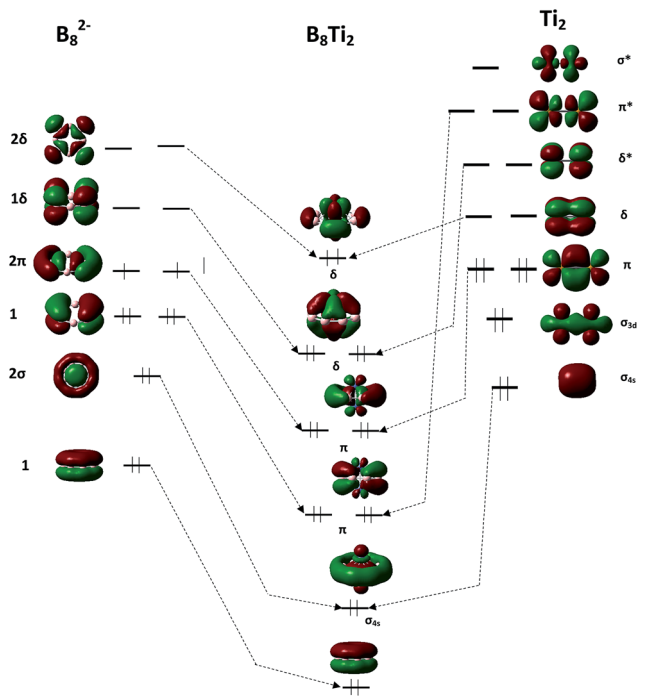

Fig. 3 Orbital interaction diagram of the Ni_2 dimer with the B_8^{2-} string.

Table 6 Orbital configurations of the bimetallic boron cycles considered

Cluster	Orbital configuration
$B_8Sc_2^{2-}$	$(\sigma_{4s})^2(\pi^*)^4(\pi)^4(\delta^*)^4$
$B_8Ti_2^{2-}$	$(\sigma_{4s})^2(\pi^*)^4(\pi)^4(\delta^*)^4(\delta)^2$
B_7NSc_2	$(\sigma_{4s})^2(\pi^*)^2(\pi)^2(\pi^*)^2(\pi)^2(\delta^*)^4$
B_7NTi_2	$(\pi^*)^2(\sigma_{4s})^2(\pi^*)^2(\pi)^4(\delta^*)^4(\sigma_{3d})^2$
$B_6C_2Sc_2$	$(\sigma_{4s})^2(\pi)^2(\pi^*)^2(\pi)^2(\pi^*)^2(\delta^*)^4(\sigma_{3d})^0$
$B_6C_2Ti_2$	$(\sigma_{4s})^2(\pi)^2(\pi^*)^2(\pi)^2(\pi^*)^2(\delta^*)^4(\sigma_{3d})^2$

Fig. 4 displays a correlation diagram of three isoelectronic bimetallic boron cycles $B_8Ti_2^{2-}$, $B_6C_2Ti_2$ and B_7NTi_2. As expected, the doubly degenerate levels of the $B_8Ti_2^{2-}$ cycle including the π, π* and δ* are now split into two separate levels in both $B_6C_2Ti_2$ and B_7NTi_2 cycles. Due to the influence of the more electronegative C and N atoms, the energy of the σ_{4s}, π*, π, δ* and δ levels of $B_6C_2Ti_2$ and B_7NTi_2 become higher than those of the $B_8Ti_2^{2-}$. Overall, the orbital interactions demonstrate that the high thermodynamic stability of bimetallic boron cycles is a consequence of two factors, namely, (i) the empty levels of B_8^{2-} involving 2π, 1δ and 2δ are occupied, and (ii) the bonding and anti-bonding MOs of M_2 are involved in stabilizing interactions with the levels of the disk B_8^{2-}, which invariably enhance the stability of the resulting clusters. As a consequence, the $B_8M_2^{0/2-}$, B_7NM_2 and $B_6C_2M_2$ clusters are stabilized within the bimetallic cyclic motif.

3.5 An analysis of the electron distribution

In order to explore further the chemical bonding phenomena, an analysis of the electron density using the electron localization indicator (ELI-D) technique[56] is performed, and the resulting partition of the densities is shown in Fig. 5. A similar localization domain pattern is thus observed for all bimetallic clusters considered. The di-synaptic basin V(B,B) is found for two B atoms of the B_8 ring in both $B_8Sc_2^{2-}$ and $B_8Ti_2^{2-}$, therefore the B atoms connect with each other *via* the classical 2e–2c bonds, and the latter go around the B_8 planar ring. For B_7NM_2, it has two localization domains located between N dopant and two B atoms yielding two 2e–2c bonds of the N with B atoms. The same behavior is observed in the mixed carbon–boron $B_6C_2M_2$ in which the C dopants connect with other B atoms by formation of 2e–2c bonds, as reflected by the presence of the V(C,B) basins. No localization domain, located in the regions between the metal M and the planar rings involving B_8, B_7N and B_6C_2, is observed, indicating a certain ionic character of the M–X bond with X = B, C and N. The localization centered on the M–M bonding is observed only at lower bifurcation values, due to their large radii. However, this does not imply that there is no direct M–M bonding.

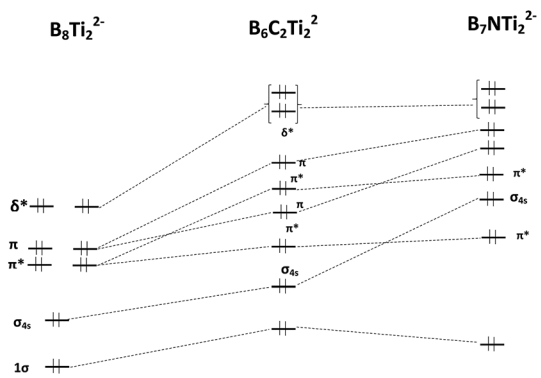

Fig. 4 Orbital correlation diagram for the $B_8Ti_2^{2-}$, $B_6C_2Ti_2$ and B_7NTi_2 clusters.

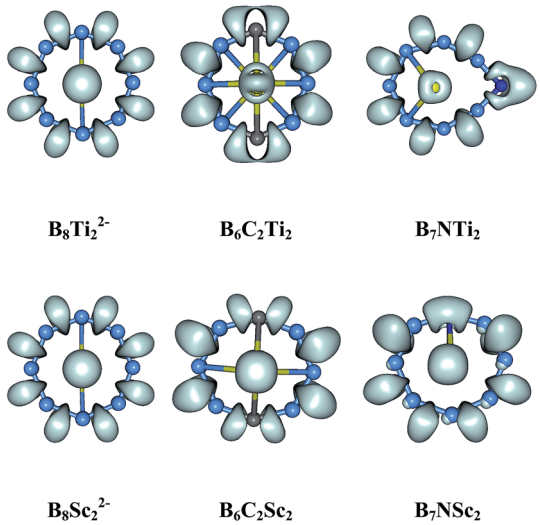

Fig. 5 The ELI_D isosurface maps obtained at the bifurcation value of 1.4 for the $B_8M_2^{2-}$, $B_6C_2M_2$ and B_7NM_2 bimetallic cyclic boron clusters, based on densities obtained at the TPSSh/cc-pVTZ level.

3.6 The aromaticity

The aromatic property of the bimetallic boron cycles considered is now analyzed using the ring current concept, which arises from a magnetic response of the electron density of the whole system. The magnetic response can be partitioned in terms of MO contributions. The contribution of each MO to the total ring current can be calculated, and thereby the participation of each MO to the aromatic character of the whole cluster can be established. The current density maps of both π and σ systems of electrons are produced on the B_8, B_6C_2 and B_7N molecular planes. Fig. 6 displays the ring current flows of the π, σ and total (involving π and σ electrons) for the bimetallic boron cycles, in their molecular plane. The ring current density maps of the π and σ orbitals are illustrated in Fig. 7.

All boron cycles containing the Sc-dopant, including $B_8Sc_2^{2-}$, $B_6C_2Sc_2$ and B_7NSc_2, exhibit a diatropic current density for both π and σ systems of electrons (Fig. 6a). A similar character is identified for both $B_8Ti_2^{2-}$ and B_7NTi_2 structures whose diatropic ring current maps are observed for both π and σ electrons (Fig. 6b). Therefore they can be classified as having a double π and σ aromaticity, according to the magnetic criteria. For the neutral $B_6C_2Ti_2$ cluster, the ring current of π electrons is of diatropic nature in magnetic response, whereas its σ electrons produce a complicated ring current map. Therefore, the aromatic character of $B_6C_2Ti_2$ will be considered in a following section on the basis of MO contributions.

It is important to consider the contribution of each MO to ring current maps, in such a way that its participation to the aromaticity can be revealed. Each of the bimetallic boron cycles $B_8M_2^{2-}$, B_7NM_2 and $B_6C_2M_2$ has 10 π electrons that populate the π* and δ* levels, and the MO-34. As a result, they can be classified as aromatic species, consistent with the classical $(4N+2)$ Hückel electron count. For a more complete understanding, the ring current maps of their π-MOs are calculated and

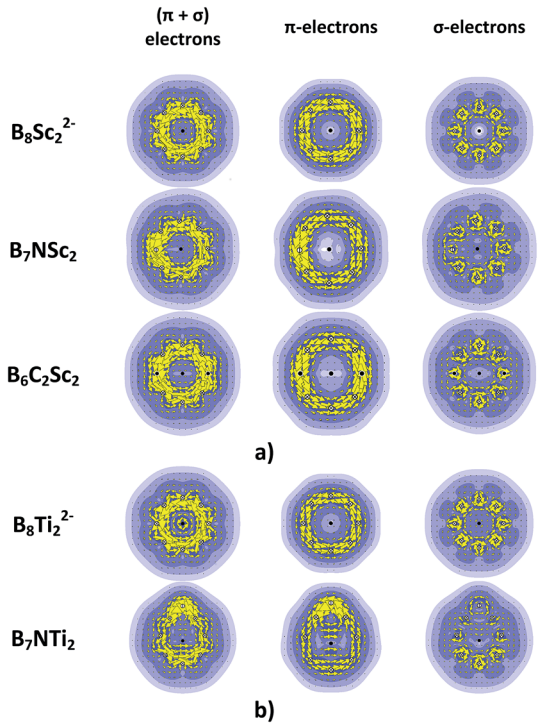

Fig. 6 The total, π and σ ring current maps of isoelectronic systems $B_8M_2^{2-}$, B_7NM_2 and $B_6C_2M_2$ clusters with M = Sc, Ti (B3LYP/6-311G(d)).

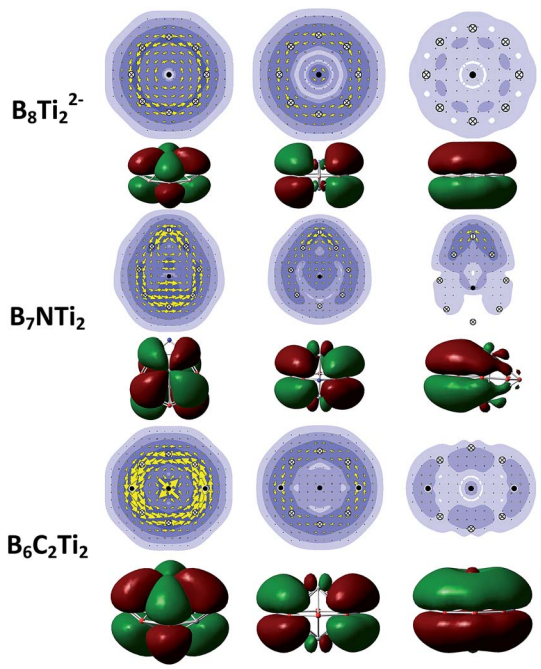

Fig. 7 The ring current maps of π-MOs of $B_8Ti_2^{2-}$, B_7NTi_2 and $B_6C_2Ti_2$ clusters (B3LYP/6-311G(d)).

displayed in Fig. 7 for boron cycles of Ti metal, and in Fig. S1 of the ESI† file for cycles containing Sc dopants. It is clear that the π ring current flows are mainly contributed, on the one hand, by two doubly degenerate MOs, namely the δ* and π* orbitals. On the other hand, the overlap of anti-bonding δ* and π*-MOs of the dimeric metal with δ and π levels of the disk configuration achieves the π diatropic current for bimetallic boron cycles. For σ electrons, the doubly degenerate π-MO brings in the main participation to diatropic ring current maps (Fig. 8), except for the $B_8Ti_2^{2-}$. In Sc-containing boron cycles, the six σ electrons of boron cycles populating the σ_{4s} and π levels are again consistent with indication of ring current criterion. Subsequently, the $(4N + 2)$ electron count also works for σ electrons of Sc clusters. Similar results are obtained for the $B_6C_2Ti_2$ and B_7NTi planar cycles in which the π levels give the main contribution to the ring current. The σ_{3d} MO of $B_6C_2Ti_2$ is active in the magnetic response and produces a complicated and unclear map for σ electrons. However, this MO can be ignored in the consideration of σ aromaticity due to the fact that it is mainly contributed by σ_{3d} of Ti_2 dimer, rather than a delocalized MO.

In of the $B_8Ti_2^{2-}$ cycle, there are 8 σ electrons arising from contribution of the doubly occupied δ-MO, beside the σ_{4s} and π levels, in such a way that this species can be regarded as anti-aromatic according to the $(4N + 2)$ electron count. The ring current map established for σ electrons of $B_8Ti_2^{2-}$ clearly illustrates the diatropic nature, and as a consequence, the $B_8Ti_2^{2-}$ cycle should be an aromatic species. On the other hand, the $(4N + 2)$ rule does not work in the case of $B_8Ti_2^{2-}$, simply because the δ-MO does not contribute to the ring current. Overall, the combination of the π-MOs (M_2) with π levels of the eight-membered ring does not only enhance the stability of the

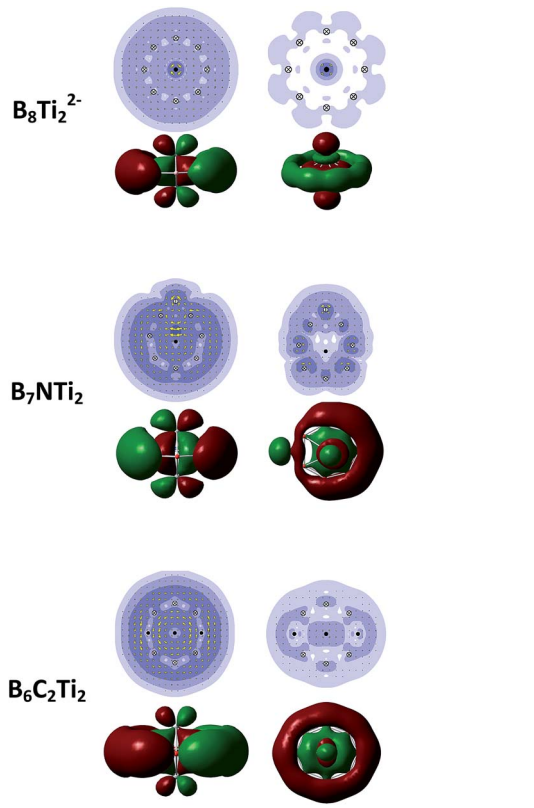

Fig. 8 The ring current maps of σ-MOs of $B_8Ti_2^{2-}$, B_7NTi_2 and $B_6C_2Ti_2$ clusters (B3LYP/6-311G(d)).

resulting MOs, but also induce an aromatic character of the bimetallic cyclic boron clusters.

4. Concluding remarks

In the present theoretical study, we investigated on the geometry, stability and aromaticity of a series of bimetal-doped boron clusters. The Sc and Ti dopants establish the bimetallic cyclic form with the eight-membered boron ring B_8^{2-} and their isoelectronic derivatives B_7N and B_6C_2, in which a perfect planar B_8^{2-}, B_7N and B_6C_2 hetero-rings are coordinated with two transition metal atoms.

The thermodynamic stability of these bimetallic boron cycles, that are the global energy minimum of the corresponding systems, can be understood as the result of a stabilizing overlap between bonding and anti-bonding MOs of M_2 with different levels of eight-membered ring. The C and N elements, which are more electronegative than the B atom, also enjoy formation of planar eight-membered ring, *via* the classical 2c–2e bonding, rather than occupy a high coordination position. The double aromaticity feature, which comprises both σ and π aromaticity, is clearly supported by the magnetic responses of the electron densities within the planar cycles. Nevertheless, such an aromatic character is not always in line with the classical electron count for both delocalized electron systems, and this suggests that the latter cannot reliably be applied to predict the aromatic character of this class of compounds.

Acknowledgements

We thank Ton Duc Thang University (TDTU-DEMASTED) for support. MTN is indebted to the KU Leuven Research Council (GOA program) and FWO-Vlaanderen for continuing support. The authors are grateful to Dr Remco Havenith at University of Groningen, for assistance with the computations of ring current maps.

References

1 B. Albert and H. Hillebrecht, *Angew. Chem., Int. Ed.*, 2009, **48**, 8640.
2 B. T. Tai, D. J. Grant, M. T. Nguyen and D. A. Dixon, *J. Phys. Chem. A*, 2010, **114**, 994.
3 B. T. Tai, N. M. Tam and M. T. Nguyen, *Chem. Phys. Lett.*, 2012, **530**, 71, http://www.sciencedirect.com/science/article/pii/S0009261412000863.
4 (*a*) B. T. Tai and M. T. Nguyen, *Phys. Chem. Chem. Phys.*, 2015, **17**, 13672; (*b*) H. T. Pham, L. V. Duong and M. T. Nguyen, *J. Phys. Chem. C*, 2014, **118**, 24181.
5 L. V. Duong, H. T. Pham, N. M. Tam and M. T. Nguyen, *Phys. Chem. Chem. Phys.*, 2014, **16**, 19470.
6 H. T. Pham, L. V. Duong, N. M. Tam, M. P. Pham-Ho and M. T. Nguyen, *Chem. Phys. Lett.*, 2014, **608**, 295.
7 B. T. Tai, N. M. Tam and M. T. Nguyen, *Theor. Chem. Acc.*, 2012, **131**, 1241.
8 A. P. Sergeeva, I. A. Popov, Z. A. Piazza, W. L. Li, C. Romanescu, L. S. Wang and A. I. Boldyrev, *Acc. Chem. Res.*, 2014, **47**, 1349.
9 T. B. Tai and M. T. Nguyen, *Chem. Commun.*, 2015, **51**, 7677.
10 Z. A. Piazza, H. S. Hu, W. L. Li, Y. F. Zhao, J. Li and L. S. Wang, *Nat. Commun.*, 2013, **5**, 3113.
11 J. Lv, Y. Wang, L. Zhu and Y. Ma, *Nanoscale*, 2014, **6**, 11692.
12 T. B. Tai and M. T. Nguyen, *Nanoscale*, 2015, **7**, 331.
13 H. J. Zhai, Y. F. Zhao, W. L. Li, Q. Chen, H. Bai, H. S. Hu, Z. A. Piazza, W. J. Tian, H. G. Lu, Y. B. Wu, Y. W. Mu, G. F. Wei, Z. P. Liu, J. Li, S. D. Li and L.-S. Wang, *Nat. Chem.*, 2014, **6**, 732.
14 T. B. Tai and M. T. Nguyen, *Chem. Commun.*, 2016, **52**, 1653.
15 H. J. Zhai, A. N. Alexandrova, K. A. Birch, A. I. Boldyrev and L. S. Wang, *Angew. Chem., Int. Ed.*, 2003, **42**, 6004.
16 H. L. Yu, R. L. Sang and Y. Y. Wu, *J. Phys. Chem. A*, 2009, **113**, 3382.
17 J. Hou, Q. Duan, J. Quin, X. Shen, J. Zhao, Q. Liang, D. Jiang and S. Gao, *Phys. Chem. Chem. Phys.*, 2015, **17**, 9644.
18 Z. Pu, K. Ito, P. v. R. Schleyer and Q. S. Li, *Inorg. Chem.*, 2009, **48**, 10679.
19 K. Ito, Z. Pu, Q. S. Li, P. v. R. Schleyer and Q. S. Li, *Inorg. Chem.*, 2008, **47**, 10906.
20 L. M. Wang, W. Huang, B. B. Averkiev, A. I. Boldyrev and L. S. Wang, *Angew. Chem., Int. Ed.*, 2007, **46**, 4550.
21 B. B. Averkiev, D. Y. Zubarev, L. M. Wang, W. Huang, L. S. Wang and A. I. Boldyrev, *J. Am. Chem. Soc.*, 2008, **130**, 9248.
22 T. R. Galeev, W. L. Li, C. Romanescu, I. Černušák, L. S. Wang and A. I. Boldyrev, *J. Chem. Phys.*, 2012, **137**, 234306.
23 B. B. Averkiev, L. M. Wang, W. Huang, L. S. Wang and A. I. Boldyrev, *Phys. Chem. Chem. Phys.*, 2009, **11**, 9840.
24 L. Guennic, H. Jiao, S. Kahlal, J. Y. Saillard, J. F. Halet, S. Ghosh, M. Shang, A. M. Beatty, A. L. Rheingold and T. P. Fehlner, *J. Am. Chem. Soc.*, 2004, **126**, 3203.
25 S. Ghosh, A. M. Beatty and T. P. Fehlner, *J. Am. Chem. Soc.*, 2001, **123**, 9188.
26 B. P. T. Fokwa and M. Hermus, *Angew. Chem., Int. Ed.*, 2012, **51**, 1702.
27 T. H. Pham and M. T. Nguyen, *Phys. Chem. Chem. Phys.*, 2015, **17**, 17335.
28 T. B. Tai and M. T. Nguyen, *J. Chem. Theory Comput.*, 2011, **7**, 1119.
29 J. M. Tao, J. P. Perdew, V. N. Staroverov and G. E. Scuseria, *Phys. Rev. Lett.*, 2003, **91**, 146401.
30 H. T. Pham, L. V. Duong, B. Q. Pham and M. T. Nguyen, *Chem. Phys. Lett.*, 2013, **577**, 32.
31 J. P. Perdew, K. Burke and M. Ernzerhof, *Phys. Rev. Lett.*, 1996, **77**, 3865.
32 J. P. Perdew, K. Burke and Y. Wang, *Phys. Rev. B: Condens. Matter Mater. Phys.*, 1996, **54**, 16533.
33 I. Valencia and M. Castro, *Phys. Chem. Chem. Phys.*, 2010, **12**, 7545.
34 H. Akeby and L. G. M. Pettersson, *J. Mol. Spectrosc.*, 1993, **159**, 17.
35 M. Moskowits, D. P. DiLella and W. Limm, *J. Chem. Phys.*, 1984, **80**, 626.

36 M. Doverstål, L. Karlsson, B. Lindgren and U. Sassenberg, *Chem. Phys. Lett.*, 1997, **270**, 273.
37 M. Doverstål, B. Lindgren, U. Sassenberg, A. Arrington and M. D. Morse, *J. Chem. Phys.*, 1992, **97**, 7087.
38 C. Cosse, M. Fouassier, T. Mejean, M. Tranwuille, D. P. DiLella and M. Moskowits, *J. Chem. Phys.*, 1980, **73**, 6076.
39 K. A. Gingerich, *Faraday Symp. Chem. Soc.*, 1980, **14**, 109.
40 L. M. Russon, S. A. Heidecke, M. K. Birke, J. Conceicao, M. D. Morse and P. B. Armentrout, *J. Chem. Phys.*, 1994, **100**, 4747.
41 M. S. Gordon, J. S. Binkley, J. A. Pople, W. J. Pietro and W. J. Hehre, *J. Am. Chem. Soc.*, 1983, **104**, 2797.
42 K. D. Dobbs and W. J. Hehre, *J. Comput. Chem.*, 1987, **8**, 861.
43 K. Raghavachari, J. S. Binkley, R. Seeger and J. A. Pople, *J. Chem. Phys.*, 1980, **72**, 650.
44 P. J. Hay, *J. Chem. Phys.*, 1977, **66**, 4377.
45 J. R. Cheeseman, J. A. Montgomery, T. Vreven, K. N. Kudin, J. C. Burant, J. Millam, *et al.*, *Gaussian 09 Revision: B.01*, Gaussian, Inc., Wallingford, CT, 2009.
46 P. Lazzeretti, M. Malagoli and R. Zanasi, SYSMO package, Technical Report "Sistemi Informatici e Calcolo Parallelo", CNR Italy (1991). Research Report number 1/67. Additional routines by P. W. Fowler, E. Steiner, R. W. A. Havenith and A. Soncini.
47 R. W. A. Havenith and P. W. Fowler, *Chem. Phys. Lett.*, 2007, **449**, 347.
48 M. F. Guest, *et al.*, *Mol. Phys.*, 2005, **103**, 719, Gamess-UK.
49 R. Zanasi, *J. Chem. Phys.*, 1996, **105**, 1460.
50 P. Lazzeretti, M. Malagoli and R. Zanasi, *Chem. Phys. Lett.*, 1994, **220**, 299.
51 K. B. Wiberg, *Tetrahedron*, 1968, **24**, 1083.
52 I. Mayer, *J. Comput. Chem.*, 2007, **28**, 204.
53 R. L. John and B. Davis, *Chem. Rev.*, 2002, **102**, 2431.
54 F. A. Cotton and D. G. Nocera, *Acc. Chem. Res.*, 2000, **33**, 483.
55 T. B. Tai, V. T. T. Huong and M. T. Nguyen, *Top. Heterocycl. Chem.*, 2014, **38**, 161.
56 M. Kohout, F. R. Wanger and Y. Grin, *Int. J. Quantum Chem.*, 2006, **106**, 1499.